ACS Catalysis

Research Article

pubs.acs.org/acscatalysis

Mononuclear Zeolite-Supported Iridium: Kinetic, Spectroscopic, Electron Microscopic, and Size-Selective Poisoning Evidence for an Atomically Dispersed True Catalyst at 22 °C

Ercan Bayram,[†] Jing Lu,[‡] Ceren Aydin,[‡] Alper Uzun,[‡,∥] Nigel D. Browning,[‡,§,¶] Bruce C. Gates,*[,‡] and Richard G. Finke*[,†]

[†]Department of Chemistry, Colorado State University, Fort Collins, Colorado 80523, United States

[‡]Department of Chemical Engineering and Materials Science, University of California, One Shields Avenue, Davis, California 95616, United States

[§]Physical and Life Sciences Directorate, Lawrence Livermore National Laboratory, 700 East Avenue, Livermore, California 94550, United States

Supporting Information

ABSTRACT: This work addresses the question of what is the true catalyst when beginning with a site-isolated, atomically dispersed precatalyst for the prototype catalytic reaction of cyclohexene hydrogenation in the presence of cyclohexane solvent: is the atomically dispersed nature of the zeolite-supported, $[Ir(C_2H_4)_2]$/zeolite Y precatalyst retained, or are possible alternatives including Ir_4 subnanometer clusters or larger, $Ir(0)_n$, nanoparticles the actual catalyst? Herein we report the (a) kinetics of the reaction; (b) physical characterizations of the used catalyst, including extended X-ray absorption fine structure spectra plus images obtained by high-angle annular dark-field scanning transmission electron microscopy, demonstrating the mononuclearity and site-isolation of the catalyst; and the (c) results of poisoning experiments, including those with the size-selective poisons $P(C_6H_{11})_3$ and $P(OCH_3)_3$ determining the location of the catalyst in the zeolite pores. Also reported are quantitative poisoning experiments showing that each added $P(OCH_3)_3$ molecule poisons one catalytic site, confirming the single-metal-atom nature of the catalyst and the lack of leaching of catalyst into the reactant solution. The results (i) provide strong evidence that the use of a site-isolated $[Ir(C_2H_4)_2]$/zeolite Y precatalyst allows a site-isolated $[Ir_1]$/zeolite Y hydrogenation catalyst to be retained even when in contact with solution, at least at 22 °C; (ii) allow a comparison of the solid−solution catalyst system with the equivalent one used in the solid−gas ethylene hydrogenation reaction at room temperature; and (iii) illustrate a methodology by which multiple, complementary physical methods, combined with kinetic, size-selective poisoning, and quantitative kinetic poisoning experiments, help to identify the catalyst. The results, to our knowledge, are the first identifying an atomically dispersed, supported transition-metal species as the catalyst of a reaction taking place in contact with solution.

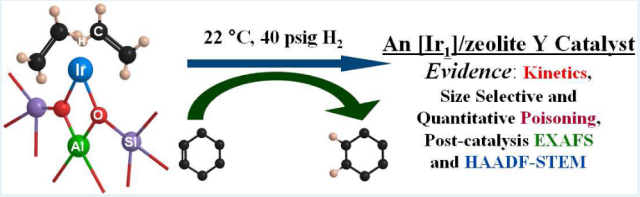

KEYWORDS: *catalysis, mononuclear, atomically dispersed, HAADF-STEM, EXAFS, kinetics, quantitative poisoning*

INTRODUCTION

Identification of the catalytically active species in a given catalytic system is a forefront research topic in catalysis[1−6] since the nature of the true catalyst—to be distinguished from the precatalyst—determines the catalytic activity, selectivity, and stability as well as the recovery, regeneration, and poisoning properties of the catalyst. Knowledge of the true catalyst is also essential for obtaining the *strongest possible*, composition-of-matter patents. Because the catalytically active species may be a small minority of those formed from the precatalyst, they can be challenging to identify.[1]

Among the simplest of supported catalysts are those consisting of mononuclear metal complexes on oxides or zeolites; they are an important class of industrial catalyst, finding application for olefin polymerization (Cr/SiO_2, for example[7]) and for olefin epoxidation (silicalite with Ti in the framework as the catalytic sites[8]). The topic of catalysis by supported mononuclear noble-metal and other complexes has drawn wide recent attention since researchers have come to recognize that such supported single-metal complexes offer previously unanticipated catalytic properties,[9−11] for example, for the water-gas shift reaction.[12,13]

Subtle control of the catalytic properties of supported metal complexes can be exerted when the complexes are converted into small clusters and, further, into metal nanoparticles. For example, mononuclear iridium complexes can be reversibly

Received: June 9, 2012
Revised: July 21, 2012
Published: August 14, 2012

converted into Ir_4 clusters by treatment in H_2 at 80 °C,[14] and under more severe conditions (i.e., at 400 °C for 8 h under 1 bar H_2), these clusters are converted into 1-nm-diameter nanoparticles.[15] The catalytic activity for ethylene hydrogenation increases markedly with increasing nuclearity of the supported species.[15]

In recent work, one of our groups focused on structural characterization of well-defined, mononuclear iridium species supported on a zeolite, namely $[Ir(C_2H_4)_2]$/zeolite Y.[16,17] Extended X-ray absorption fine structure (EXAFS) and infrared (IR) spectroscopies were employed to show[14,18] that a mononuclear zeolite Y-supported iridium complex, abbreviated as Ir_1/zeolite Y, is the only detectable form of iridium produced from the precatalyst during ethylene hydrogenation at 25 °C in ethylene-H_2 mixtures in a plug-flow reactor. Hence, mononuclear Ir_1/zeolite Y was proposed as the leading candidate for the catalytically active species (i.e., appropriately ligated and as opposed to higher-nuclearity species).[18] However, remaining to be accomplished are additional experiments specifically designed to check the nature of the kinetically dominant catalyst, including poisoning experiments and post-catalysis, atomic-resolution electron microscopy to test for the formation of species other than the mononuclear Ir_1/zeolite Y in that gas−solid reaction system.

In work at Colorado State University (CSU), one of our groups has endeavored to determine the identities of catalysts and determine whether the catalysis is homogeneous or heterogeneous.[1−3,19−22] For example,[23] these questions were addressed for benzene hydrogenation at 100 °C and 50 atm initial H_2 pressure when the catalyst precursor was $[RhCp^*Cl_2]_2$. In that study, in operando-EXAFS results showed that 98 ± 2% of the total, initial rhodium mass from $[RhCp^*Cl_2]_2$ transforms into ligated Rh_4 clusters (with the average formula of $Rh_4Cp^*_{2.4}Cl_4H_c$) as the only (±2%) detectable rhodium species. Quantitative 1,10-phenanthroline poisoning studies with both model, polyethyleneglycol-dodecyl ether hydrosol-stabilized $Rh(0)_n$ nanoparticles (poisoned by 0.12 ± 0.02 equiv of 1,10-phenanthroline per total equiv of Rh present) and the Rh_4 clusters (poisoned by 4.0 ± 0.4 equiv of 1,10-phenanthroline per total equiv of Rh present) provided strong evidence that the Rh_4 clusters observed via in operando-EXAFS spectroscopy are the catalytically active species for benzene hydrogenation. This conclusion followed even though control experiments with the model, 2−3 nm diameter $Rh(0)_n$ nanoparticles revealed that if even 1.4% of the total Rh mass had evolved to such $Rh(0)_n$ nanoparticles, then they would have been kinetically competent to carry 100% of the observed catalytic activity. This example illustrates how trace species, formed under the reaction conditions from the precatalyst, can be highly active catalysts.

In the work reported herein, we combine the complementary approaches of the two research groups to answer the question of (i) "who is the true catalyst?" when beginning with the site-isolated, $[Ir(C_2H_4)_2]$/zeolite Y precatalyst, now investigating prototype reaction of cyclohexene hydrogenation *in contact with the cyclohexane solution* in a batch reactor at 22 °C. Additional questions addressed in this work include: (ii) What are the dominant forms of the catalyst evolving from the solid $[Ir(C_2H_4)_2]$/zeolite Y in contact with solution, and does the presence of the liquid phase change that speciation when compared to our previously reported investigation of the gas−solid reaction, vide supra?[18] (iii) Are, as expected, a synergistic combination of spectroscopy and microscopy, accompanied by measurements of kinetics and quantitative catalyst poisoning experiments, required en route to identification of the true catalyst?[23] In addition, (iv) we sought to determine how well characterizations of the working catalyst determined by kinetics meshed with the information available from post-catalysis ex-situ EXAFS and electron microscopy.

One other premise of the work reported herein is that investigations of the formation of supported catalytic species, in contact with solution, may help transfer the synthetic and mechanistic insights that have emerged from investigations of nanoparticle formation in contact with solution[24−27] to the synthesis of improved supported nanoparticle catalysts. We regard $[Ir(C_2H_4)_2]$/zeolite Y as an especially valuable starting material because of the mononuclear nature and structural uniformity of $[Ir(C_2H_4)_2]$/zeolite Y, as well as the information now available characterizing its reactivity.[18,28,29] Now, by investigating the reactivity of $[Ir(C_2H_4)_2]$/zeolite Y in contact with solution, we have the first opportunity[24] to examine and compare gaseous vs liquid environments for reactions, vide infra, for this well-characterized, site-isolated, atomically dispersed, zeolite Y-supported precatalyst system.

Here we present an investigation of the cyclohexene hydrogenation catalyst when beginning with $[Ir(C_2H_4)_2]$/zeolite Y in contact with cyclohexane solution at 22 ± 0.1 °C and 40 ± 1 psig (ca. 2.7 atm) initial H_2 partial pressure. The key experiments consist of (i) kinetics, (ii) post-catalysis EXAFS spectroscopy and high-angle annular dark-field scanning transmission electron microscopy (HAADF-STEM), (iii) size-selective poisoning experiments with $P(C_6H_{11})_3$ and $P(OCH_3)_3$, and (iv) quantitative kinetic poisoning experiments with $P(OCH_3)_3$. The results, taken together, provide a strong if not compelling case against higher-nuclearity species, but for a mononuclear $[Ir_1]$/zeolite Y catalyst.

For clarity of presentation, we begin with experimental details, reporting experiments performed at the University of California, Davis (UCD), Colorado State University (CSU), the National Synchrotron Light Source (NSLS), and the Stanford Synchrotron Radiation Lightsource (SSRL).

EXPERIMENTAL METHODS AND DATA ANALYSIS

Materials and General Considerations. *Precatalyst Synthesis at UCD.* Precatalyst syntheses and handling were performed with the exclusion of moisture and air. The highly dealuminated HY zeolite (DAY zeolite) (Zeolyst International, CBV760), with a Si:Al atomic ratio of approximately 30, was calcined in O_2 at 500 °C for 4 h and evacuated for 16 h at 500 °C. After calcination, the zeolite was isolated and stored in an argon-filled drybox (MBraun, with an H_2O concentration <0.5 ppm and an O_2 concentration <5 ppm as monitored by VAC monitors equipped with LM-H_2O-A and LM-O_2-A alarms). *n*-Pentane (Fisher, 99%) was dried and purified by column chromatography (Grubbs apparatus, MBraun SPS) in the presence of argon.

Cyclohexene Hydrogenation and Poisoning Experiments at CSU. Unless indicated otherwise, all manipulations were performed under N_2 in a Vacuum Atmospheres drybox. Oxygen concentrations were continuously maintained in the drybox at ≤5 ppm, monitored by a Vacuum Atmospheres O_2 monitor. Unless noted otherwise, all solvents, compounds, and other materials mentioned below were stored in the drybox. Cyclohexane (99.5%, anhydrous), $P(OCH_3)_3$ (≥99.999%), and $P(C_6H_{11})_3$ (≥94%) were purchased from Aldrich and used as received. Cyclohexene (99%, inhibitor free) was

dx.doi.org/10.1021/cs300366w | ACS Catal. 2012, 2, 1947−1957

distilled over sodium metal under argon or purified in a MicroSolv solvent purification system (Innovative Technology) equipped with an activated γ-Al_2O_3 column under N_2. H_2 gas was purchased from General Air (>99.5%) and was passed through a Trigon Moisture Trap and a Trigon Technologies Oxygen/Moisture Trap to remove O_2 and H_2O followed by a Trigon Technologies High Capacity Indicating Oxygen Trap. The conversion of cyclohexene to cyclohexane was verified by ^{1}H NMR spectra of a sample prepared by adding a drop of the resultant product solution into 1 mL of CD_2Cl_2 (Cambridge Isotope Laboratories) followed by examination with a Varian INOVA-300 instrument, 300.115 MHz for ^{1}H (cyclohexene: 5.5 ppm (m), 2 ppm (m), 1.6 ppm (m); cyclohexane: 1.4 ppm (s)).

Sample Transport Between UCD and CSU. The exclusion of air/O_2 was accomplished by careful handling of the samples in argon or N_2 atmosphere dryboxes. That is, the samples to be shipped to either CSU (for cyclohexene hydrogenation and poisoning experiments) or to UCD (for HAADF-STEM analysis and for preparation for transport to a synchrotron for EXAFS spectroscopy) were prepared in a drybox. The samples were placed into a stainless-steel Swagelok vacuum tube, the ends were clamped together, sealed with O-rings, and shipped to the other laboratory or to the synchrotron, where the vacuum tube was opened in a drybox and prepared for the reactions or analyses, vide infra.

Synthesis and Characterization of [Ir(C$_2$H$_4$)$_2$]/Zeolite Y Containing 1 wt % Iridium. [Ir(C$_2$H$_4$)$_2$(acac)] (acac = $CH_3COCH_2COCH_3$) was synthesized and characterized at UCD as described elsewhere[30] and slurried in dried *n*-pentane at ice temperature with the calcined zeolite powder in a Schlenk flask. The stirred slurry was warmed to room temperature and, after one day, the solvent was removed by evacuation over another day. The resultant solid, [Ir(C$_2$H$_4$)$_2$]/zeolite Y containing 1 wt % iridium, was characterized[16] by EXAFS, IR, and NMR spectroscopies and was stored in an argon-filled drybox.

Catalytic Hydrogenation Apparatus. The hydrogenation reactions at CSU were carried out with the previously described, custom-built pressurized hydrogenation apparatus that allows monitoring of the pressure in real time (±0.01 psig) as H_2 is consumed during the cyclohexene hydrogenation reactions.[31−33] The apparatus consists of a Fischer−Porter (F−P) bottle connected via its Swagelok TFE-sealed Quick Connects to a hydrogenation line and an Omega D1512 10 V A/D converter with an RS-232 connection to a PC interface via LabView ver. 8.2. Once the pressure-transducer H_2 uptake data were obtained, the data were converted to cyclohexene loss data via the known 1:1 H_2:cyclohexene stoichiometry.[19]

Procedure for Cyclohexene Hydrogenation Reaction under Standard Conditions Starting with [Ir(C$_2$H$_4$)$_2$]/Zeolite Y. To begin with, at CSU, 25 ± 1 mg of [Ir(C$_2$H$_4$)$_2$]/zeolite Y (1 wt % Ir) in a drybox was weighed in a 2-dram glass vial and then transferred into a new 22 × 175 mm Pyrex culture tube containing a new 5/16 × 5/8-in. Teflon-coated stir bar. Cyclohexane (2.5 mL) and cyclohexene (0.5 mL) were added via separate gastight syringes. The culture tube was sealed inside the F−P pressure bottle and brought outside of the drybox. The F−P bottle was placed into a constant-temperature circulating bath at 22 ± 0.1 °C and attached via Swagelok TFE-sealed Quick-Connects to the hydrogenation line (which had already been evacuated for at least 30 min to remove trace oxygen and water), then refilled with purified H_2 at 40 ± 1 psig (ca. 2.7 atm). Stirring at 600 rpm was started, the F−P bottle was purged 10 times with H_2 (5 s between purges), and the reaction was started and t = 0 designated. The foregoing statement defines what is referred to below as a Standard Conditions cyclohexene hydrogenation reaction experiment.

When the H_2 uptake ceased according to the PC interfaced monitoring, the F−P bottle was disconnected from the hydrogenation line, the remaining H_2 pressure was released, and the F−P bottle was transferred back into the drybox. The resultant solution in the culture tube was transferred into a new 20-mL scintillation vial with a new 5/16 × 5/8-in. Teflon-coated stir bar and dried under vacuum for 8 h. This sample was sealed in a stainless-steel Swagelok-equipped vacuum tube sealed with O-rings, brought out of the drybox, and shipped to UCD for characterization investigations. The above Standard Conditions cyclohexene hydrogenation reaction was repeated five times, yielding the same initial rates and total reaction times within ±10%.

A test for H_2 gas-to-solution mass-transfer limitations (MTL) was performed by changing the stirring speed (450, 600, and 1000 rpm) for a Standard Conditions cyclohexene hydrogenation reaction, essentially as before.[21] Specifically, a Standard Conditions cyclohexene hydrogenation reaction yielded the same initial H_2 uptake rates within ±10% experimental error at these stirring speeds (see the Supporting Information for the data). This result indicates negligible H_2 gas-to-solution MTLs.

Calculations according to the Thiele model[34] were performed to check for diffusion limitations within the pores of the catalyst. The results indicate a negligible diffusion resistance (the Thiele modulus is approximately 1; see the Supporting Information). Consequently, we infer that the rates of the catalytic reaction are without significant transport limitations and characterize the intrinsic chemistry. Details of the calculations are given in the Supporting Information.

Kinetic Data Treatment: Initial Rate Method. Initial rates were calculated from either the H_2 partial pressure loss vs time or the cyclohexene concentration vs time data by employing the initial rate method described elsewhere.[35] The resultant data were fit to a third-degree polynomial equation via GraphPad Prism software (version 5 for Mac OS X, GraphPad Software, San Diego, California U.S.A., www.graphpad.com) with R^2 > 0.990. Then, the derivative of the third-degree polynomial was taken at time t = 0 yielding the initial rate (the t^1 term of the polynomial).[35]

Experiments Demonstrating Linear Dependence of Reaction Rate on Mass of Catalyst and Zero-Order Dependences on [*Cyclohexene*]$_{initial}$ and [H_2]$_{initial}$. The details of these experiments at CSU are provided in the Supporting Information. Briefly, zero-order dependencies were observed for both [*cyclohexene*]$_{initial}$ and the initial H_2 partial pressure. The rates of the catalytic reaction are reported as turnover frequencies (TOFs; rate per Ir atom per unit time) on the basis of the following three lines of evidence: since the initial rate was found to be proportional to the mass of catalyst, since the intrapore diffusion resistance was found to be negligible, and since the evidence which follows demonstrates that the catalyst was atomically dispersed.

Subsequent Cyclohexene Hydrogenation. The details of this experiment are provided in the Supporting Information. Briefly, the total reaction times and initial rates were compared for an initial cyclohexene hydrogenation run and a subsequent cyclohexene hydrogenation run using that same catalyst

solution, but with additional cyclohexene added before the start of the second run: about 12 h and $-\{d[cyclohexene]/dt\}_{initial}$ = 0.30 M/h for the first run vs about 14 h and $-\{d[cyclohexene]/dt\}_{initial}$ = 0.25 M/h for the second run. The data representing the second run were corrected for the changed volumes, 3.0 mL (first run) to 3.5 mL (second run) by multiplying the initial rate observed in the second run by 1.16 to obtain the indicated $-\{d[cyclohexene]/dt\}_{initial}$ = 0.25 M/h for the second run, a correction consistent with the observed, overall first-order rate law, vide infra.

X-ray Absorption Spectroscopy (XAS). The X-ray absorption spectra were recorded at X-ray beamline X18-B at NSLS at Brookhaven National Laboratory (BNL) and at beamline 4-1 at SSRL. The storage ring electron energy and ring current were ∼3 GeV and 200−300 mA, respectively. Si(111) and Si(220) double-crystal monochromators were used at BNL and SSRL, respectively. Each monochromator was detuned to 80% of maximum intensity to reduce the interference of higher harmonics in the X-ray beam.

To minimize the exposure to air and moisture, each powder sample was placed in a glass vial and sealed with Parafilm inside the argon-filled drybox. Each glass vial was placed into a stainless-steel Swagelok-equipped vacuum tube sealed with O-rings for transfer to the synchrotron. The mass of each sample (approximately 0.3 g) was chosen to give an absorbance between 1.5 and 3.0 measured at 50 eV above the Ir L_{III} edge (11215 eV). In an N_2-filled glovebox at the synchrotron, each sample was pressed into a wafer and mounted in a cell for transmission spectroscopy[36] and maintained under vacuum (at a pressure of 10^{-7} kPa) at liquid-nitrogen temperature during the data collection. X-ray intensity data were collected in transmission mode by use of ion chambers mounted on each end of the sample cell.

EXAFS Data Analysis. The X-ray absorption edge energy was calibrated with the measured signal of a platinum foil (scanned simultaneously with the sample) at the Pt L_{III} edge, which was taken to be the inflection point at 11564 eV. The data were normalized by dividing the absorption intensity by the height of the absorption edge.

Analysis of the EXAFS data was carried out with the software ATHENA of the IFEFFIT[37,38] package and the software XDAP developed by Vaarkamp et al.[39] Each spectrum that was analyzed was the average of four spectra. ATHENA was used for edge calibration and deglitching. XDAP was used for background removal, normalization, and conversion of the data into an EXAFS (χ) file. A "difference-file" technique for shell isolation was applied with XDAP for determination of optimized fit parameters. A second-order polynomial was fit to the data in the pre-edge region and subtracted from the entire spectrum in each analysis. The functional that was minimized, and the function used to model the data, are given elsewhere.[40] The background was subtracted by using cubic spline routines. Reference backscattering phase shifts were calculated with the software FEFF7[41] from crystallographic data. $[Ir(C_2H_4)_2(acac)]$, which has a known crystal structure[30] incorporating π-bonded ethylene ligands and a bidentate acac ligand, was used as the reference for Ir−$O_{support}$, Ir−C, Ir−O_{long}, and Ir−C_{long} (the latter two being Ir−O and Ir−C contributions at distances longer than bonding distances); Ir−Al alloy[42] (Al_3Ir) was used for Ir−Al contributions, and iridium metal[42] was used for Ir−Ir first- and second-shell contributions. For a summary of the Ir-backscatterer distances in the reference compounds used for EXAFS analysis, see the Supporting Information, Table SI-2.

Iterative fitting was done in R (distance) space with the Fourier-transformed χ data until optimum agreement was attained between the calculated k^0-, k^1-, k^2-, and k^3-weighted EXAFS data and each postulated model (k is the wave vector). The number of parameters used in the fitting was always less than the statistically justified number, computed with the Nyquist theorem:[43] $n = (2\Delta k\Delta r/\pi) + 1$, where Δk and Δr are the k and r ranges used in the fitting, respectively, and r is the interatomic distance.

In the EXAFS analysis, various combinations of plausible absorber−backscatterer contributions (Ir−$O_{support}$, Ir−C, Ir−Al, Ir−C_{long}, and Ir−Ir) were fitted initially, which led to a narrowed list of candidate models on the basis of the goodness-of-fit and the overall fit, in both k space and R space. The detailed fitting parameters of the final candidate models of each sample are summarized in Supporting Information, Table SI-1, and the corresponding fits for each model analysis are given in the Supporting Information, Figures SI-3, SI-4, and SI-5.

To further examine the fitting parameters and to compare candidate models, a "difference-file" technique was applied by using the software XDAP,[36] in which the calculated EXAFS contribution from each individual Ir-backscatterer contribution was compared with the data in R space (calculated from subtracting all the other calculated Ir-backscatterer contributions from the experimental overall contributions). The best model should give not only good overall fits in both k space and R space, but should also fit each individual contribution well.

We emphasize that the contributions are very weak for those Ir-backscatterer combinations with distances that are longer than bonding distances, so that it is difficult to distinguish one from another (e.g., to distinguish between Ir−C_{long} and Ir−O_{long}). Hence, those contributions are assigned only tentatively, and the errors characterizing those shells are greater than those stated below for other shells. Details of all the EXAFS data analyses and fitting for each model are provided in the Supporting Information.

HAADF-STEM: Sample Handling, Instrumentation, and Analysis. To minimize the exposure to air and moisture, powder samples (prepared at UCD or shipped from CSU in a stainless-steel Swagelok vacuum tube, vide supra) were loaded onto a lacey carbon, 300-mesh copper grid (Ted-Pella) in the argon-filled drybox. The grid was packed in an Eppendorf tube and sealed with Parafilm inside the drybox. Each Eppendorf tube was placed into a stainless-steel Swagelok vacuum tube sealed with O-rings for transfer to the microscope facility. There, an argon-filled glovebag (Glas-Col) was purged five times with ultrahigh-purity argon (Praxair, grade 5.0), and the TEM grid was loaded onto the TEM holder under the blanket of flowing argon in the glovebag. The TEM holder was then inserted into the microscope under flowing argon, with a time of possible exposure to air of <5 s. Prior to imaging of a sample, the aberration corrector was aligned with a Pt/Ir-on-holey-carbon standard sample (SPI Supplies) until atomic resolution of the metal particles was achieved and the lattice spacings of the metals were confirmed.

Images of the samples were obtained with a JEOL JEM-2100F electron microscope at UCD. The microscope was equipped with a field emission gun (FEG), operating at 200 kV, with a CEOS hexapole probe (STEM) aberration corrector. An HAADF detector with a collection semiangle of 75−200 mrad and a probe convergence semiangle of 17.1 mrad was used to

capture the images. To minimize the artifacts in the images caused by beam damage, the microscope was aligned for one region of the sample, and then the beam was shifted to a neighboring region for a quick image acquisition: 5 s for a 512 × 512 pixel size.

Poisoning Experiments with Phosphine and Phosphite. *Size-Selective Poisoning Studies Using $P(OCH_3)_3$ and $P(C_6H_{11})_3$.* At CSU, two aforementioned cyclohexene hydrogenation reactions beginning with $[Ir(C_2H_4)_2]$/zeolite Y were repeated at 22 ± 0.1 °C, with one change: in two separate experiments, 1 equiv of $P(OCH_3)_3$ or $P(C_6H_{11})_3$ per equiv of total iridium present (1.3×10^{-6} mol) was added to the initial reaction solutions in the separate experiments. For the $P(OCH_3)_3$ poisoning experiment, 0.15 μL of $P(OCH_3)_3$ was added via a 1-μL syringe to the initial 2.5 mL of cyclohexane plus 0.5 mL of cyclohexene solution mixed with 25 ± 1 mg of $[Ir(C_2H_4)_2]$/zeolite Y. For the $P(C_6H_{11})_3$ poisoning experiment, a stock solution was prepared by dissolving 0.4 mg of $P(C_6H_{11})_3$ in 10 mL of cyclohexane. Then, 0.1 mL of this stock solution (i.e., 1 equiv of $P(C_6H_{11})_3$ per mol of Ir present) was added via a 1 mL syringe to the initial 2.5 mL of cyclohexane along with 0.5 mL of cyclohexene solution, all mixed with 25 ± 1 mg of $[Ir(C_2H_4)_2]$/zeolite Y. Each size-selective poisoning experiment was repeated three times, yielding the same values of the initial reaction rate within ±10%.

Quantitative $P(OCH_3)_3$ Poisoning Experiments. Three separate experiments were carried out at CSU as described in the aforementioned Standard Conditions reaction starting with $[Ir(C_2H_4)_2]$/zeolite Y, except that a prechosen amount of $P(OCH_3)_3$ poison was added as follows. Specifically, a Standard Conditions reaction was started at 22 ± 0.1 °C; after 5 h, the F−P bottle was removed from the line, vented, and taken into the drybox where, then, one of 0.1, 0.4, or 0.7 equiv (1.3×10^{-7}, 5.2×10^{-7}, 9.1×10^{-7} mol, respectively) of $P(OCH_3)_3$ per equiv of total Ir were added in 3 separate, but otherwise identical, experiments. The addition of $P(OCH_3)_3$ was accomplished using a stock solution prepared by adding 0.15 μL of $P(OCH_3)_3$ to 0.1 mL of fresh cyclohexane via a 1-μL syringe. Then, 0.01, 0.04, and 0.07 mL (or, equally, 10, 40, and 70 μL via 100-μL syringe, respectively) of this stock solution was added to the F−P bottle that had been brought back into the drybox for the respective 0.1, 0.4, and 0.7 equiv of $P(OCH_3)_3$ poisoning experiments. (For each trial, a new stock solution was prepared.) The F−P bottle was then resealed, taken out of the drybox, and reconnected to the hydrogenation line. Stirring at 600 rpm was restarted, the F−P bottle was then again purged 10 times with H_2 (5 s between purges), and then refilled with 40 ± 1 psig of H_2. At this point, collection of pressure versus time data was continued (ignoring the ∼1 h gap required for the procedure). Each quantitative poisoning experiment with $P(OCH_3)_3$ was repeated three times, yielding the same total reaction time within ±10%.

An additional control experiment, repeating the same procedure but without added $P(OCH_3)_3$, showed no change in the catalytic activity. Hence, the observed decrease in catalytic activity upon addition of $P(OCH_3)_3$ is inferred to have been caused by the addition of $P(OCH_3)_3$ and not any aspect of the ∼1 h procedure required for that addition.

RESULTS AND DISCUSSION

Synthesis, Characterization, and Structure of the $[Ir(C_2H_4)_2]$/Zeolite Y Precatalyst. The $[Ir(C_2H_4)_2]$/zeolite Y precatalyst was synthesized as reported previously[16] and as summarized in the Experimental Section. Briefly, $[Ir(C_2H_4)_2(acac)]$[30] was slurried with highly dealuminated zeolite Y (Si/Al atomic ratio = 30) to form $[Ir(C_2H_4)_2]$/zeolite Y. The structure of the supported iridium complex was elucidated on the basis of multiple complementary techniques including EXAFS, IR, and NMR spectroscopies, STEM, mass spectrometry of effluent gases formed during sample treatments, and density functional theory.[16,17] The iridium in this well-defined supported complex has been shown to incorporate two π-bonded ethylene ligands and two Ir−O bonds to the zeolite, Figure 1.[16] The individual iridium complexes are site-isolated and well-separated from each other, with the loading corresponding to approximately 1 Ir atom per 12 zeolite supercages; the zeolite incorporates approximately one Al site per supercage.[16]

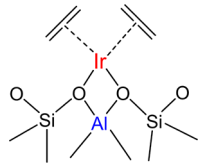

Figure 1. Schematic representation of the structure of $[Ir(C_2H_4)_2]$/zeolite Y prepared by the reaction of $[Ir(C_2H_4)_2(acac)]$ with highly dealuminated (Si/Al = 30) zeolite Y.[16] Each Ir atom is π-bonded to two ethylene ligands and anchored to the support by two Ir−O bonds, as in the precursor $[Ir(C_2H_4)_2(acac)]$.[16]

Kinetics of Cyclohexene Hydrogenation Reaction Starting with $[Ir(C_2H_4)_2]$/Zeolite Y in Contact with Cyclohexane Solvent at 22 °C and 40 psig (ca. 2.7 atm) Initial H_2 Partial Pressure. Cyclohexene hydrogenation was employed as a prototypical test reaction[19,25,26] and was performed using cyclohexane as the solvent. A slurry consisting of 25 ± 1 mg of $[Ir(C_2H_4)_2]$/zeolite Y in cyclohexene (0.5 mL) plus cyclohexane (2.5 mL) was stirred (600 rpm) at 22 ± 0.1 °C and 40 ± 1 psig initial H_2 partial pressure. The progress of the reaction was monitored by the pressure loss via a PC-interfaced pressure transducer reporting precise, ±0.01 psig, pressure data. The hydrogenation reaction in the batch reactor started immediately, without a detectable induction period, and took ∼12 h to go to completion, Figure 2. The cyclohexane end product and 100% reaction (i.e., the lack of detectable starting cyclohexene) were confirmed by ^{1}H NMR spectra of an aliquot of the liquid product. Four repetitions of the experiment yielded data which agreed within ±10% with those shown in Figure 2. The reaction slurry retained its pale-dirty-gray color throughout the reaction; no darkening—that is, no brown or darker material characteristic of metal nanoparticle formation[1]—was observed. The absence of an induction period and the lack of a color change or darkening of the solution are consistent with the hypothesis that the starting mononuclear iridium complex anchored to zeolite Y is the catalyst—with one or more of the ethylene ligands in the $[Ir(C_2H_4)_2]$/zeolite Y precatalyst presumably being replaced by cyclohexene and/or hydrogen, vide infra.

In the presence of an excess of cyclohexene reactant relative to catalyst, and at a constant initial H_2 partial pressure, the initial rate of the reaction, $-\{d[H_2]/dt\}_{initial}$, is proportional to the mass of precatalyst (as shown in Supporting Information, Figure SI-1a). The initial rate at constant initial (total) precatalyst was then used, in a series of experiments varying the concentration of cyclohexene (at constant initial H_2 partial

dx.doi.org/10.1021/cs300366w | ACS Catal. 2012, 2, 1947−1957

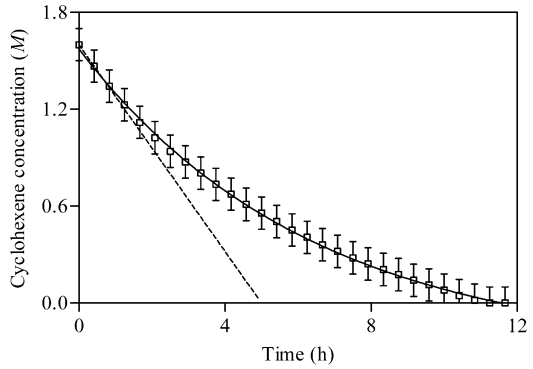

Figure 2. Hydrogenation of cyclohexene in presence of cyclohexane solvent under the Standard Conditions (22 ± 0.1 °C and 40 ± 1 psig initial H_2 partial pressure) and starting with 25 mg (1 wt % Ir) $[Ir(C_2H_4)_2]$/zeolite Y (□). The error bars depict an estimated ±5% absolute error based on repetitive runs (which indicate that the absolute [*cyclohexene*] values are no more precise than the ±5% shown). The initial rate,[45] $-\{d[cyclohexene]/dt\}_{initial}$ = 0.30 *M*/h, determined as the slope of the tangent line at time = 0, was determined from a third-order polynomial fit (solid line) with R^2 = 0.999. This rate corresponds to a TOF of 3.2 × 10^{-25} mol × (Ir atom × s)$^{-1}$. The observed rate constant is then k_{obs}= 1 × 10^{-5} mol × (g of catalyst × s)$^{-1}$ for the 25 mg of $[Ir(C_2H_4)_2]$/zeolite Y catalyst, corresponding to $TOF_{initial}$ = 0.20 ± 0.03 molecules × (Ir atom × s)$^{-1}$. For clarity, only one of every ten data points collected and fit is shown.

pressure) and then varying the initial H_2 partial pressure (at constant $[cyclohexene]_{initial}$), to determine the reaction orders in the initial [*cyclohexene*] and in the initial H_2 partial pressure, respectively. The initial rate data reveal zero-order dependencies on both the $[cyclohexene]_{initial}$ and on the $\{H_2$ partial pressure$\}_{initial}$. Specifically, the data from a Standard Conditions cyclohexene hydrogenation experiment provide an initial rate value, $-\{d[cyclohexene]/dt\}_{initial}$ of 0.30 *M* × h^{-1}, that yields a rate constant of k_{obs} = 1 × 10^{-5} mol × (g of catalyst × s)$^{-1}$ for 25 mg of $[Ir(C_2H_4)_2]$/zeolite Y catalyst, corresponding to a $TOF_{initial}$ = 0.20 ± 0.03 molecules × (Ir atom × s)$^{-1}$.[44] A footnote summarizes why the kinetic plots are concave up, reflecting changes from the initial zero-order dependencies on [*cyclohexene*] and the H_2 partial pressure as the reactants are consumed in the batch reactor.[45]

A second, repeat cyclohexene hydrogenation reaction was performed with the catalyst slurry produced by the first run, as summarized in the Supporting Information. Briefly, once the first, Standard Conditions cyclohexene hydrogenation was completed (via H_2 uptake cessation and ^{1}H NMR analysis), the F−P bottle and its reaction solution were transported back into the drybox, 0.5 mL of fresh cyclohexene added, the F−P bottle removed from the drybox and reattached to the hydrogen line, and a second, repeat cyclohexene hydrogenation run started. The plot of the cyclohexene loss is given in the Supporting Information, Figure SI-2b; those data reveal: (i) no induction period; (ii) no darkening of the reaction solution; and (iii) an initial rate $-\{d[cyclohexene]/dt\}_{initial}$ = 0.25 *M*/h (Supporting Information, Figure SI-2b) that is 16% less than that of the first run $-\{d[cyclohexene]/dt\}_{initial}$ = 0.30 *M*/h (Figure 2 and Supporting Information, Figure SI-2a), with a total reaction time of 14 h, slightly longer than the total reaction time of the first run of 12 h.[46] The lack of an induction period (during which a new catalyst could have been formed) is consistent with the hypothesis that a mononuclear Ir_1/zeolite Y species is the catalyst.

All the data presented to this point are consistent with the hypothesis that a mononuclear iridium species is the catalyst. However, an alternative hypothesis not yet disproven is that larger iridium species, such as Ir_4 subnanometer clusters,[14] or larger Ir_n nanoparticles, could have formed so quickly that no induction period would be evident, an interpretation that also requires that those putative Ir_4 or larger Ir_n species be active catalysts (as they are for ethylene hydrogenation[15]). Hence, EXAFS spectroscopy and HAADF-STEM were employed to characterize the nuclearity of the post-catalysis iridium species.

Post-Catalysis EXAFS Analysis of the Resultant Iridium Species and Comparison to the Starting Material, $[Ir(C_2H_4)_2]$/Zeolite Y. After a Standard Conditions cyclohexene hydrogenation reaction, the resultant sample was dried under vacuum for 8 h in a drybox and transported in the absence of air and moisture as detailed in the Experimental section for characterization by EXAFS spectroscopy and HAADF-STEM.[47]

For the analysis of the EXAFS data characterizing the sample, several candidate models were investigated that were selected on the basis of the expected and plausible contributions. Relevant literature here is the characterization by EXAFS spectroscopy of the precatalyst $[Ir(C_2H_4)_2]$/zeolite reported previously.[48] For what follows, we emphasize that attempts were made to include Ir−Ir contributions in each model to test for the presence/absence of iridium clusters. These models (I, II, and III) included the following respective contributions: Ir−$O_{zeolite}$, Ir−C, Ir−Al, and Ir−C_{long}; Ir−$O_{zeolite}$, Ir−C, Ir−Al, and Ir−O_{long}; and Ir−$O_{zeolite}$, Ir−C, and Ir−Al (and each of these was also tested with inclusion of an Ir−Ir contribution).

None of the models tested gave evidence of an Ir−Ir contribution in any *k*-weighting. Each of the three models (I−III) provides a satisfactory fit of the data on the basis of the overall fitting statistics, with good overall fits in both *k* space and *R* space (Supporting Information, Figures SI 3−5). Each indicates a mononuclear zeolite-supported iridium complex with hydrocarbon ligands bonded to zeolite support oxygen atoms. Both Model I and Model II provide good individual shell fits for all contributions. However, Model II was rejected because the coordination numbers for the Ir−$O_{support}$ and Ir−C contributions are unrealistically high (breaking the 18-e^- rule for the supported iridium complex) (Supporting Information, Table SI-1). Moreover, the coordination number characterizing the Ir−Al contribution in Model II is also unrealistically high for the zeolite, which has a Si/Al atomic ratio of 30:1 (Supporting Information, Table SI-1). Model III was rejected because of the poor individual shell fit for the Ir−Al contribution and a relatively poor overall fit in *R* space in comparison with Models I and II.

Thus, of the three models, Model I (Table 1) was selected as the preferred model, yielding the most realistic coordination numbers for iridium. This model fits the data excellently, as illustrated by the comparisons shown in Figure 3.

As shown in Table 1, according to this recommended model, coordination numbers (CN) of 4.9 and 3.6 were found for the Ir−C and Ir−C_{long} contributions, respectively, indicating the presence of hydrocarbons bonded to the iridium. The EXAFS data are not sufficient to determine the identities of the hydrocarbon ligands, but they are consistent with the expected ligands, which include cyclohexene, ethylene, ethyl, or a combination of these, as just one set of plausible possibilities.[49]

The assignments of the Ir−$O_{zeolite}$ and Ir−Al contributions are supported by the reported synthesis chemistry.[16,28,50]

Table 1. Summary of the EXAFS Data at the Ir L_{III} Edge Characterizing the Starting Complex, $[Ir(C_2H_4)_2]$/Zeolite Y,[48] and the Post-Catalysis Iridium Species Characterizing the Recommended Model[a]

	EXAFS parameters				
sample	absorber–backscatterer pair	N	R (Å)	$10^3 \times \Delta\sigma^2$ (Å^2)	ΔE_0 (eV)
$[Ir(C_2H_4)_2]$/zeolite Y[b]	Ir–$O_{zeolite}$	2.0	2.12	13	−5.1
	Ir–C	4.1	2.10	10	−2.2
	Ir–Al	1.1	3.02	6.8	−7.9
	Ir–Ir	*c*	*c*	*c*	*c*
post-catalysis iridium sample	Ir–$O_{zeolite}$	2.1	2.18	5.4	−8.0
	Ir–C	4.9	2.09	11	−6.6
	Ir–Al	1.1	3.01	0.6	−2.2
	Ir–C_{long}	3.6	2.98	1.0	−6.7
	Ir–Ir	*c*	*c*	*c*	*c*

[a]See the Supporting Information for details. Notation: N, coordination number; R, distance between absorber and backscatterer atoms; $\Delta\sigma^2$, variance in the absorber–backscatterer distance; ΔE_0, inner potential correction. Error bounds (accuracies) characterizing the structural parameters are estimated to be as follows: N, ± 20%; R, ± 0.02 Å; $\Delta\sigma^2$, ± 20%; and ΔE_0, ± 20%. [b]See the details elsewhere.[48] [c]Contribution not detected.

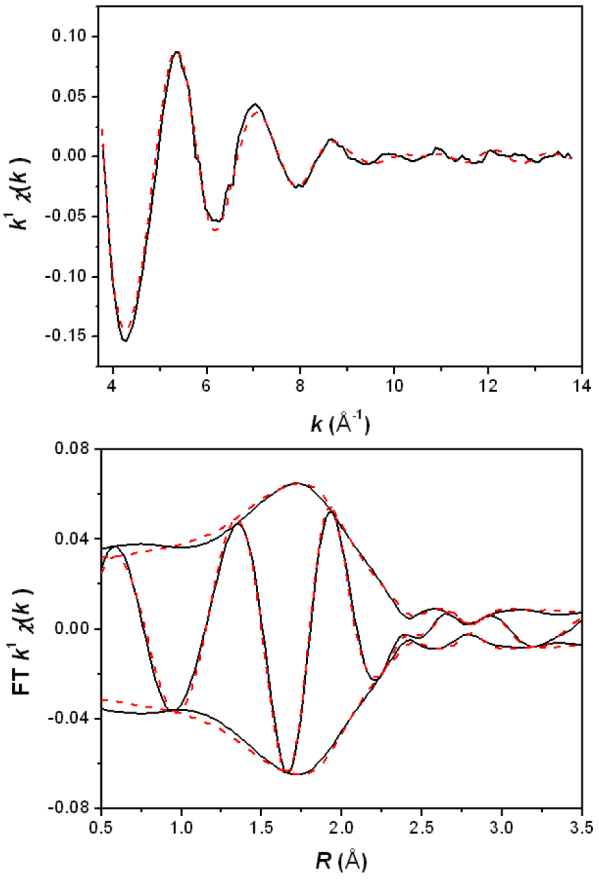

Figure 3. EXAFS analysis of the post-catalysis iridium species. *Top*: k^1-weighted EXAFS function, χ (solid line), and sum of the calculated contributions (dashed line). *Bottom*: k^1-weighted imaginary part and magnitude of the Fourier transform of the data (solid line) and sum of the calculated contributions (dashed line). Both EXAFS function and the Fourier transform show excellent fits. See the Experimental Section for a detailed summary of the EXAFS analysis method.

Briefly, the $[Ir(C_2H_4)_2(acac)]$ precursor undergoes ligand exchange with the zeolite, which takes place preferentially at the Al^- sites where the precursor reacts with the proton and releases the acac ligands as Hacac. As a result, the zeolite support replaces the bidentate acac ligand and bonds to the cationic iridium complex by two Ir–$O_{support}$ bonds at the Al^- sites. The Ir–$O_{support}$ distances detected by EXAFS spectroscopy are 2.12 and 2.18 Å for the initially prepared and post-catalysis samples, respectively. These distances are typical for bonding of six group-9 metals to oxygen atoms on the surfaces of metal oxides and zeolites.[51,52]

Moreover, the Ir–$O_{support}$ distances characterizing both the precatalyst and the post-catalysis samples (2.12 and 2.18 Å, respectively), are markedly different from the crystallographically determined Ir–O distance characterizing the precursor $[Ir(C_2H_4)_2(acac)]$ (2.04 Å),[30] consistent with the replacement of the acac ligand with a zeolite ligand as a result of the adsorption.

The EXAFS data show no detectable changes in the metal–support Ir–$O_{zeolite}$ and Ir–Al contributions (i.e., no detectable change in their respective CNs) as a result of exposure of the catalyst to the reacting solution. This result, and the lack of detectable Ir–Ir interactions, are consistent with the kinetic data, vide supra, as well as the hypothesis that mononuclear Ir_1/zeolite Y is the catalyst. In other words, a comparison of the EXAFS data for the post catalysis product with that of the $[Ir(C_2H_4)_2]$/zeolite Y starting material,[48] Table 1, is supportive of the inference that the cyclohexene hydrogenation catalyst is the Ir_1/zeolite Y site shown in Figure 1, but with a different ligand environment around iridium as expected for the catalyst in the presence of a solution of cyclohexene, cyclohexane, and H_2.

Post-Catalysis XANES Analysis of the Resultant Iridium Species and Comparison to the Starting Material, $[Ir(C_2H_4)_2]$/Zeolite Y, and Ir_4 Clusters, Ir_4/Zeolite Y. Figure 4 shows the XANES spectra at the Ir L_{III} edge characterizing the initially prepared $[Ir(C_2H_4)_2]$/zeolite Y, the used catalyst, and, for comparison, zeolite Y-supported Ir_4 clusters (prepared from $[Ir(C_2H_4)_2]$/zeolite Y in 1 bar H_2 at 353 K for 1 h, as described previously[18,29]). The spectra show changes in the near edge features after exposure of the sample

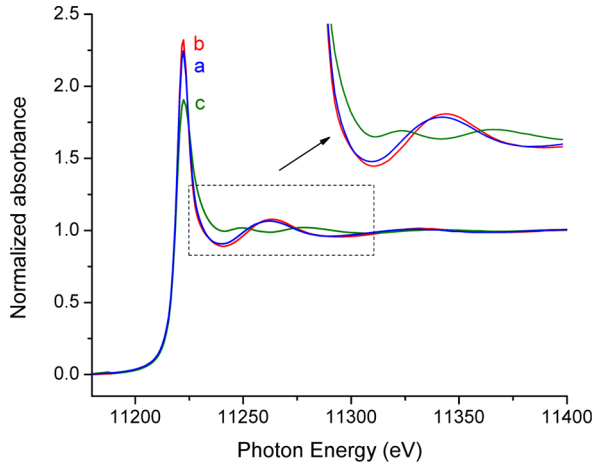

Figure 4. Normalized XANES spectra at the Ir L_{III}-edge characterizing (a) $[Ir(C_2H_4)_2]$/zeolite Y, (b) catalyst after use in kinetics experiment, and (c) Ir_4/zeolite Y (prepared from $[Ir(C_2H_4)_2]$/zeolite Y in 1 bar H_2 flow at 353 K for 1 h, as described previously[18,29]).

dx.doi.org/10.1021/cs300366w | ACS Catal. 2012, 2, 1947–1957

to cyclohexene hydrogenation reaction conditions, reflecting changes in the ligand environment of the iridium. The changes in the white line intensity as a result of this exposure are too small to provide much information, but the fact that the white line intensities of the supported iridium catalyst before and after reaction are both significantly higher than that of supported Ir_4 clusters shows that such clusters were not present in any detectable amount in either the used catalyst or the precatalyst. Thus, these comparisons are consistent with the EXAFS results, and indicate the presence of a cationic iridium complex—and the absence of iridium clusters.

Post-Kinetics HAADF-STEM Analysis of the Resultant Iridium Species and Comparison to Starting Material, $[Ir(C_2H_4)_2]$/Zeolite Y. The same post-catalysis iridium sample, as well as the starting supported iridium complex $[Ir(C_2H_4)_2]$/zeolite Y, were imaged with HAADF-STEM, Figure 5. The

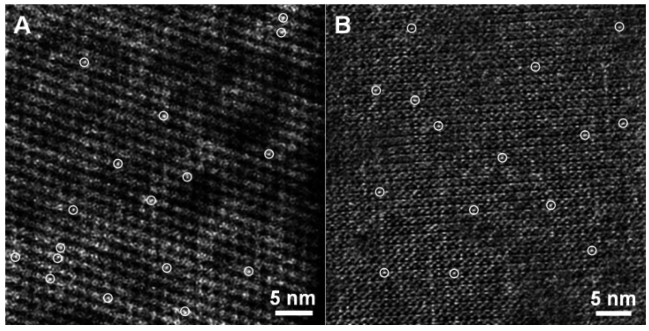

Figure 5. HAADF-STEM images of (A) initially prepared $[Ir(C_2H_4)_2]$/zeolite Y, and (B) the post-catalysis sample. Bright features are the site-isolated, single Ir atoms supported in zeolite Y. A few, representative single Ir atoms are circled to aid their visualization.

atomic-resolution images show the presence of isolated Ir atoms (a few are circled in the images). No iridium clusters or larger iridium nanoparticles are detectable either in the images of the initial $[Ir(C_2H_4)_2]$/zeolite Y or in the post-catalysis sample. In short, the images indicate only mononuclear iridium species.

Overall, the post-catalysis HAADF-STEM results are in agreement with the post-catalysis EXAFS spectra—as well as all the other results presented so far—in supporting the inference of mononuclear Ir_1/zeolite Y as the true catalyst. The kinetic poisoning data provided in the next section provide additional, very strong if not compelling evidence for both an Ir_1 catalyst, as well as for its intrazeolitic pore location.

Size-Selective Poisoning Experiments with the Bulky Phosphine, $P(C_6H_{11})_3$, and the Smaller Phosphite, $P(OCH_3)_3$. One additional, alternative hypothesis for the identity of the catalyst not yet disproven is that small amounts of iridium might have leached from the zeolite into solution. If, for example, even 1% of the total iridium had been extracted into solution but was 1000-fold more active catalytically than the zeolite-bound Ir_1, then that leached species in this hypothetical example would be responsible for ~90% of the observed catalytic reaction rate.

Hence, to test this alternative hypothesis, the size-selective properties of the zeolite were exploited in quantitative catalyst poisoning experiments. These potential ligands were chosen for their ability to bond strongly to iridium and, thereby, to poison the catalyst if they can access it.[1] Relevant here is that $P(C_6H_{11})_3$, with its three bulky cyclohexyl groups, has a diameter of ~10 Å[53] and a cone angle of 170°,[54] and is therefore too large to enter the supercages of zeolite Y via the pore apertures, which have diameters of only 7.4 Å.[55] In contrast, $P(OCH_3)_3$, with its three methoxy groups, has a diameter of ~5 Å[53] and a cone angle of 107°,[54] so that it can pass through the zeolite pores.

Experimentally and under our Standard Conditions for cyclohexene hydrogenation at 22 ± 0.1 °C and 40 ± 1 psig initial H_2 partial pressure, the addition of 1.0 equiv of $P(C_6H_{11})_3$ per equiv of total iridium present *did not affect the catalytic activity* within experimental error. The cyclohexene hydrogenation activity started immediately without an observable induction period, and again the catalytic reaction was completed in ~12 h, Figure 6a, as confirmed by ^1H NMR

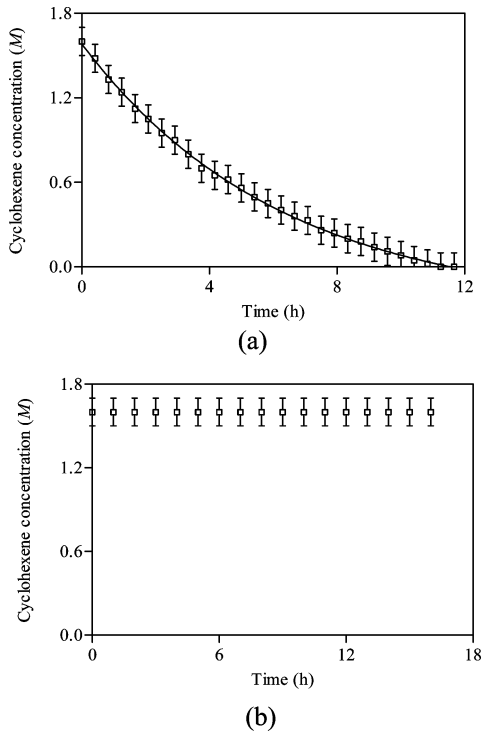

Figure 6. Cyclohexene hydrogenation kinetics at 22 ± 0.1 °C: (a) After the addition of 1 equiv (per mole of iridium) of $P(C_6H_{11})_3$ (□); the polynomial fit (solid line), R^2 = 0.999, yields an initial rate of $-\{d[cyclohexene]/dt\}_{initial}$ = 0.28 *M*/h, within experimental error of the initial rate of 0.30 *M*/h shown in Figure 2. For clarity, only one of every 10 data points is shown. (b) Results of a separate experiment showing the complete deactivation of the catalyst following the addition of 1 equiv of $P(OCH_3)_3$ (per mole of iridium), all under the otherwise identical Standard Conditions. For clarity, only one of every 20 data points is shown. In both Figures 5a and 5b, the error bars depict an estimated ±5% absolute error based on repetitive runs. These selective poisoning experiments provide strong evidence that all of the detectable catalysis occurs in the zeolite Y pores.

spectra of the liquid product. The $TOF_{initial}$ is the same within error as that observed without the poison: ($TOF_{initial}$ = 0.18 ± 0.03 molecules × (Ir atom × s)$^{-1}$ *with* 1.0 equiv of $P(C_6H_{11})_3$ per mole of iridium vs $TOF_{initial}$ = 0.20 ± 0.03 molecules × (Ir atom × s)$^{-1}$ *without* $P(C_6H_{11})_3$).

Whereas the nonpoisoning by $P(C_6H_{11})_3$ is by itself a negative result, in contrast, the addition of 1.0 equiv of $P(OCH_3)_3$ per equiv of total iridium led to a complete deactivation of the catalyst for more than 15 h, after which the

dx.doi.org/10.1021/cs300366w | *ACS Catal.* 2012, 2, 1947−1957

experiment was stopped, Figure 6b. Taken together, the results of the size-selective poisoning experiments with phosphorus-containing compounds—the smaller ($P(OCH_3)_3$) being a poison and the larger ($P(C_6H_{11})_3$) not—provide prima facie evidence that all of the detectable catalytically active iridium is confined within the zeolite pores.

These results also demonstrate the advantage of using a zeolite as a catalyst support when the goal is to identify the catalytically active species—size-selective poisoning experiments are then available to assist in identification and location of the catalyst.[56]

Quantitative $P(OCH_3)_3$ Poisoning Experiments. Although the hypothesis that a supported mononuclear iridium species, Ir_1/zeolite Y, is the catalyst is consistent with all the data presented so far, one more alternative hypothesis which has not yet been unequivocally ruled out is that fast formation of small amounts of highly active, higher-nuclearity iridium species (such as Ir_4 clusters or larger Ir_n nanoparticles) occurs in the supercages of the zeolite and that these are the catalyst. According to this hypothesis, the presumed cluster or nanoparticle species would not have been observed by EXAFS spectroscopy (because of the lack of sensitivity of the method to minor components) or by HAADF-STEM, because they were somehow missed (although this is unlikely in our experience). Furthermore, the hypothetical multinuclear species would also have to be postulated to be much more active catalysts than the Ir_1 species.[15]

Hence, quantitative poisoning experiments with $P(OCH_3)_3$ were performed to test this plausible alternative hypothesis, as summarized in detail in the Experimental Section. Briefly, three separate experiments were initiated at 22 ± 0.1 °C and 40 ± 1 psig initial H_2 partial pressure. After 5 h, 0.1, 0.4, and 0.7 equiv of $P(OCH_3)_3$ (per equiv of total iridium) were added, respectively, to the reactor in the three separate experiments. The increased $P(OCH_3)_3$ poison concentration gradually slowed down the catalytic reaction, as shown in Figure 7, and 1.0 equiv of $P(OCH_3)_3$ per mole of iridium again poisoned the catalyst completely as previously observed, vide supra. Specifically, the reaction was found to take 14, 23, and 60 h to completion upon the addition of 0.1, 0.4, and 0.7 equiv of $P(OCH_3)_3$ per equiv of iridium, respectively, compared with about 12 h without any added $P(OCH_3)_3$, Figure 2.

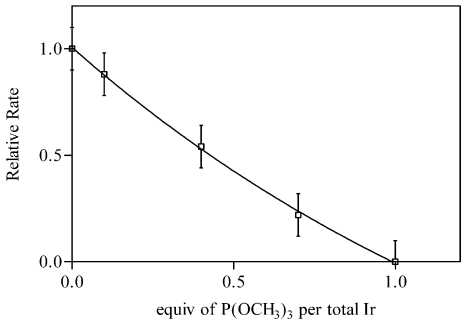

Figure 7. Results of quantitative poisoning experiments with $P(OCH_3)_3$ at 22 ± 0.1 °C under a Standard Conditions cyclohexene hydrogenation beginning with $[Ir(C_2H_4)_2]$/zeolite Y. The error bars represent a propagated, ±10% (±0.1) estimated absolute error based, as before, on the error observed in repeat runs. A gradual decrease in the activity was observed as a function of added equivalents of $P(OCH_3)_3$ per equivalent of iridium: 14, 23, and 60 h to completion upon the addition of 0.1, 0.4, and 0.7 equiv of $P(OCH_3)_3$ per equiv of iridium, respectively, compared to ∼12 h without any added $P(OCH_3)_3$ (Figure 2). Overall, 1.0 equiv of $P(OCH_3)_3$ per equiv of total iridium present completely inhibits the catalytic activity.

The key result from Figure 7 is that ∼1.0 equiv of poison, $P(OCH_3)_3$, per total equiv of iridium is required to deactivate the catalyst completely, *as expected for an Ir_1 catalyst*. Crucial here is that the required ∼1.0 equiv of poison is quite distinct from the expectation for multinuclear metal catalysts, the specific case of at least previous Ir_n nanoparticle catalysts[57] requiring only ≪1 equiv (often 0.1−0.3 equiv)[57,58] of poison per total equiv of metal present for complete deactivation. This result is as expected for nanoparticle catalysts since only a fraction of the metal atoms are exposed and catalytically active,[58] with only ∼40% of the atoms of an ∼3-nm, $Ir(0)_{\sim 900}$ nanoparticle, for example, being on the surface of the nanoparticle and thus only ∼40% even accessible. These quantitative poisoning experiments, along with all the other evidence presented to this point, provide very strong evidence that the mononuclear nature of the $[Ir(C_2H_4)_2]$/zeolite Y precatalyst is retained in a kinetically dominant, Ir_1/zeolite Y catalyst.

SUMMARY

In summary, all the available evidence—in our view the combination of the needed evidence—is strongly supportive of the inference that a mononuclear iridium complex supported within the supercages of the zeolite, $[Ir_1]$/zeolite Y, is the catalytically active species for hydrogenation of cyclohexene at 22 ± 0.1 °C and 40 ± 1 psig initial H_2 partial pressure. This inference is supported by five lines of consistent, if not compelling, evidence: (i) the lack of an observable induction period (i.e., the lack if a period during which higher-nuclearity iridium species could have been formed) and the lack of darkening of the reaction solution (which could have indicated the formation of nanoparticles); (ii) the post-catalysis, ex-situ EXAFS analysis of the resultant iridium species indicating no detectable Ir−Ir contributions, but fully consistent with mononuclear Ir_1/zeolite Y; (iii) the post-catalysis, ex-situ HAADF-STEM analysis that detected only atomically dispersed Ir_1 on the zeolite support; (iv) the results of the size-selective poisoning experiments, which are consistent only with catalysis by iridium species within the zeolite pores, and (v) the quantitative $P(OCH_3)_3$ poisoning experiments which make a strong case for a mononuclear Ir_1 catalyst, as opposed to Ir cluster (e.g., Ir_4) or Ir_n nanoparticle catalysts.

The above evidence for a zeolite-supported mononuclear iridium catalyst, for cyclohexene hydrogenation in the presence of cyclohexane solvent, closely parallels the characterization of a mononuclear, zeolite-supported Ir_1 complex as the dominant species in the presence of gas-phase ethylene and H_2 at 25 °C and 1 atm.[18] A mononuclear species was inferred to be the active catalyst in the latter case since there is spectroscopic evidence for Ir_1/zeolite along with no evidence for iridium clusters, not even the Ir_4 observed to form at the higher temperature of 80 °C.[18] In short, all the available evidence points to a consistent, clear picture of zeolite-supported Ir_1 as catalyst for either gas−solid[18] or liquid−solid hydrogenation of olefins, *at least at mild temperatures of 22−25 °C*. Thus, the presence or absence of liquid-phase cyclohexene and cyclohexane does not alter the catalytically active site at 22−25 °C.

In sum, a well-characterized, site-isolated, atomically dispersed $[Ir(C_2H_4)_2]$/zeolite Y precatalyst has been shown to evolve into an active catalyst for which arguably compelling

dx.doi.org/10.1021/cs300366w | ACS Catal. 2012, 2, 1947−1957

evidence has been collected supporting the hypothesis that the catalyst at 22−25 °C retains its atomic dispersion, Ir_1/zeolite Y. This is to our knowledge the first example for which all the evidence needed to identify an atomically dispersed, zeolite-supported transition metal species as the catalyst has been obtained.[9,11−13]

In work in progress, we raised the temperature 50 °C and investigated the present system under otherwise identical conditions. There we do detect higher-nuclearity species (experiments which also provide a check on the results reported herein, demonstrating that we would have detected such higher-nuclearity species had they been formed at 22−25 °C). Experiments are in progress to identify the kinetically dominant catalyst(s) under those higher temperature, 72 °C conditions. The results promise to yield insights into the *sintering of an initially atomically dispersed catalyst*. Hence, we are working hard to bring those results to a publishable conclusion.

■ ASSOCIATED CONTENT

Ⓢ Supporting Information

Experimental details and plots of kinetic experiments varying the $[Ir(C_2H_4)_2]$/zeolite Y, cyclohexene, and H_2 amounts and determining the corresponding initial rate changes to determine the order of reaction in each of those reactants as well as the control varying the stirring rate; Experimental details, data, and fit to third-degree polynomial of a second, repeat cyclohexene hydrogenation using the product solution plus its comparison to the first run; Details of the EXAFS data analyses with the fits of the candidate models; Tabulated Ir-backscatterer pair distances of the reference compounds used for EXAFS analysis; XANES data characterizing air-exposed catalyst; Calculation of the Thiele modulus. This material is available free of charge via the Internet at http://pubs.acs.org.

■ AUTHOR INFORMATION

Corresponding Author

*E-mail: bcgates@ucdavis.edu (B.C.G.), rfinke@lamar.colostate.edu (R.G.F.).

Present Addresses

[‖]Department of Chemical and Biological Engineering, Koc University, Rumelifeneri Yolu 34450 Sariyer, Istanbul, Turkey. [¶]Fundamental and Computational Sciences Division, Pacific Northwest National Laboratory, 902 Battelle Boulevard, Richland, WA 99352, U.S.A.

Notes

The authors declare no competing financial interest.

■ ACKNOWLEDGMENTS

This work was supported by the Department of Energy (DOE) Grant FG02-04ER15513 (J.L.), Grant DE-FG02-03ER15453 (to R.G.F. at CSU), Grant DE-FG02-03ER46057 (C.A.), and the University of California Lab Fee Program. A.U. was supported by a fellowship from Chevron. We gratefully acknowledge beam time and support of the DOE Division of Materials Sciences for its role in the operation and development of beamline X-18B at the NSLS and beamline 4-1 at SSRL. We also thank Professor Saim Özkar for valuable discussions leading to the size-selective catalyst poisoning experiments.

■ REFERENCES

(1) Widegren, J. A.; Finke, R. G. *J. Mol. Catal. A: Chem.* **2003**, *198*, 317−341.
(2) Phan, N. T. S.; Sluys, M. V. D.; Jones, C. W. *Adv. Synth. Catal.* **2006**, *348*, 609−679.
(3) Crabtree, R. H. *Chem. Rev.* **2012**, *112*, 1536−1554.
(4) Alley, W. M.; Hamdemir, I. K.; Johnson, K. A.; Finke, R. G. *J. Mol. Catal. A: Chem.* **2010**, *315*, 1−27.
(5) Dyson, P. J. *Dalton Trans.* **2003**, 2964−2974.
(6) de Vries, J. G. *Dalton Trans.* **2006**, 421−429.
(7) McDaniel, M. P. *Adv. Catal.* **2010**, *53*, 123−606.
(8) Ratnasamy, P.; Srinivas, D.; Knözinger, H. *Adv. Catal.* **2004**, *48*, 1−169.
(9) Qiao, B.; Wang, A.; Yang, X.; Allard, L. F.; Jiang, Z.; Cui, Y.; Liu, J.; Li, J.; Zhang, T. *Nat. Chem.* **2011**, *3*, 634−641.
(10) Lu, J.; Aydin, C.; Browning, N. D.; Gates, B. C. *Angew. Chem., Int. Ed.* **2012**, *51*, 5842−5846.
(11) Kyriakou, G.; Boucher, M. B.; April, D.; Jewell, A. D.; Lewis, E. A.; Lawton, T. J.; Baber, A. E.; Tierney, H. L.; Flytzani-Stephanopoulos, M.; Sykes, E. C. H. *Science* **2012**, *335*, 1209−1212.
(12) Flytzani-Stephanopoulos, M.; Gates, B. C. *Ann. Rev. Chem. Biomol. Eng.* **2012**, *3*, 545−574.
(13) Zhai, Y.; Pierre, D.; Si, R.; Deng, W.; Ferrin, P.; Nilekar, A. U.; Peng, G.; Herron, J. A.; Bell, D. C.; Saltsburg, H.; Mavrikakis, M.; Flytzani-Stephanopoulos, M. *Science* **2010**, *329*, 1633−1636.
(14) Uzun, A.; Gates, B. C. *Angew. Chem., Int. Ed.* **2008**, *47*, 9245−9248.
(15) Aydin, C.; Lu, J.; Browning, N. D.; Gates, B. C. *Angew. Chem., Int. Ed.* **2012**, *51*, 5929−5934.
(16) Uzun, A.; Bhirud, V. A.; Kletnieks, P. W.; Haw, J. F.; Gates, B. C. *J. Phys. Chem. C* **2007**, *111*, 15064−15073.
(17) Ortalan, V.; Uzun, A.; Gates, B. C.; Browning, N. D. *Nat. Nanotechnol.* **2010**, *5*, 506−510.
(18) Uzun, A.; Gates, B. C. *J. Am. Chem. Soc.* **2009**, *131*, 15887−15894.
(19) Watzky, M. A.; Finke, R. G. *J. Am. Chem. Soc.* **1997**, *119*, 10382−10400.
(20) Watzky, M. A.; Finke, R. G. *Chem. Mater.* **1997**, *9*, 3083−3095.
(21) Aiken, J. D., III; Finke, R. G. *J. Am. Chem. Soc.* **1998**, *120*, 9545−9554.
(22) Widegren, J. A.; Aiken, J. D., III; Özkar, S.; Finke, R. G. *Chem. Mater.* **2001**, *13*, 312−324.
(23) Bayram, E.; Linehan, J. C.; Fulton, J. L.; Roberts, J. A. S.; Szymczak, N. K.; Smurthwaite, T. D.; Özkar, S.; Balasubramanian, M.; Finke, R. G. *J. Am. Chem. Soc.* **2011**, *133*, 18889−18902.
(24) Mondloch, J. E.; Bayram, E.; Finke, R. G. *J. Mol. Catal. A: Chem.* **2012**, *355*, 1−38.
(25) Mondloch, J. E.; Wang, Q.; Frenkel, A. I.; Finke, R. G. *J. Am. Chem. Soc.* **2010**, *132*, 9701−9714.
(26) Mondloch, J. E.; Finke, R. G. *J. Am. Chem. Soc.* **2011**, *133*, 7744−7756.
(27) Mondloch, J. E.; Finke, R. G. *ACS Catal.* **2012**, *2*, 298−305.
(28) Lu, J.; Serna, P.; Aydin, C.; Browning, N. D.; Gates, B. C. *J. Am. Chem. Soc.* **2011**, *133*, 16186−16195.
(29) Lu, J.; Aydin, C.; Browning, N. D.; Gates, B. C. *J. Am. Chem. Soc.* **2012**, *134*, 5022−5025.
(30) Bhirud, V. A.; Uzun, A.; Kletnieks, P. W.; Craciun, R.; Haw, J. F.; Dixon, D. A.; Olmstead, M. M.; Gates, B. C. *J. Organomet. Chem.* **2007**, *692*, 2107−2113.
(31) Lin, Y.; Finke, R. G. *J. Am. Chem. Soc.* **1994**, *116*, 8335−8353.
(32) Özkar, S.; Finke, R. G. *J. Am. Chem. Soc.* **2002**, *124*, 5796−5810.
(33) Özkar, S.; Finke, R. G. *Langmuir* **2002**, *18*, 7653−7662.
(34) Bird, R. B.; Stewart, W. E.; Lightfoot, E. N. In *Transport Phenomena*; Wiley: New York, 2002.
(35) Wilkins, R. G. In *Kinetics and Mechanisms of Reactions of Transition Metal Complexes*, 2nd ed.; VCH: New York, 1991.
(36) Jentoft, M.; Deutsch, S. E.; Gates, B. C. *Rev. Sci. Instrum.* **1996**, *67*, 2111−2113.
(37) Newville, M.; Ravel, B.; Haskel, D.; Rehr, J. J.; Stern, E. A.; Yacoby, Y. *Phys. B* **1995**, *208/209*, 154−156.
(38) Newville, M. *J. Synchrotron Radiat.* **2001**, *8*, 96−100.

(39) Vaarkamp, M.; Linders, J. C.; Koningsberger, D. C. *Phys. B* **1995**, *209*, 159−160.
(40) Koningsberger, D. C.; Mojet, B. L.; van Dorssen, G. E.; Ramaker, D. E. *Top. Catal.* **2000**, *10*, 143−155.
(41) Zabinsky, S. E.; Rehr, J. J.; Ankudinov, A.; Albers, R. C.; Eller, M. J. *Phys. Rev. B.* **1995**, *52*, 2995−3009.
(42) Pearson, W. B.; Calvert, L. D.; Villars, P. In *Pearson's Handbook of Crystallographic Data for Intermetallic Phases*; American Society for Metals: Metals Park, OH, 1985.
(43) Lytle, F. W.; Sayers, D. E.; Stern, E. A. *Phys. B* **1989**, *158*, 701−722.
(44) For comparison, the initial TOF for *ethylene* hydrogenation with the catalyst formed from the same precatalyst, but in a solid−gas phase reaction, is the about 3.5 fold larger value of 0.71 molecules × (Ir atom × s)$^{-1}$, in the latter case for a feed of C_2H_4 and H_2 at partial pressures of 333 and 666 mbar, respectively, all at 25 °C and atmospheric pressure.[14]
(45) The plot in Figure 2 (and the others in the Supporting Information) are concave up; the reaction is zero order in the *initial* cyclohexene concentration and in the *initial* partial pressure of H_2. Hence, if these reaction orders pertained over the whole conversion range, then the plot would have been linear. The curvature observed instead can be rationalized by increasing orders of reaction as the reactants are depleted and, thereby and presumably, the catalyst is no longer saturated with the reactants. Relevant here is that we are monitoring the H_2 pressure loss, so that even though the reaction begins with a zero-order dependence on the initial partial H_2 pressure, at some point in the reaction the H_2 partial pressure-dependence must transition to something more like first order. Hence, the decreasing H_2 partial pressure as the reaction proceeds is expected to contribute to a decrease of the observed rate and a resultant concave-up plot as shown (the H_2 consumed under our Standard Conditions corresponds to a change in H_2 partial pressure from 40 to 25 psig, corresponding to a change in absolute pressure from about 55 to 40 psia). Also relevant is that the cyclohexene is completely used up during the reaction; hence, analogous to the above case for H_2, the dependence of the rate on cyclohexene concentration must transition from an initial zero-order dependence to something more like first order later in the reaction. The above considerations both rationalize the curvature seen in Figure 2 and related plots, and also make apparent why initial-rate kinetics have been deliberately and solely used throughout the kinetic studies.
(46) A control experiment of adding 0.5 mL of fresh cyclohexene without bringing the F-P bottle into the drybox (i.e., adding 0.5 mL of fresh cyclohexene to the solution at the end of first run under flowing H_2 gas) yielded the same initial rate within experimental error as the experiment given in the main text in which 0.5 mL of cyclohexene were added after detaching the F-P bottle, taking it into the drybox, adding the cyclohexene there, and removing the F-P reactor from the drybox, reattaching it to the hydrogen line, and starting the second cyclohexene hydrogenation. This control shows that the sample manipulation, including removing the H_2 from the catalyst, does not cause the observed slightly lower initial rate in the second hydrogenation run.
(47) We recently noted[23] the general importance of applying in-operando spectroscopy of functioning catalysts to identify where and in what form the precatalyst mass resides. However, ex-situ EXAFS and HAADF-STEM experiments were employed in this work, in significant part since samples had to be shipped between laboratories to take advantage of the specialized equipment in each laboratory. One advantage of the third-row element iridium is that the relatively strong Ir−support bond energies appear to make the samples relatively stable to ex-situ conditions and analyses. To minimize possible contamination from air/O_2, the catalysts were prepared and handled meticulously to exclude air/O_2 during the transfers between laboratories (as summarized in the Experimental Section). In addition and as a control reported in the Supporting Information, air was intentionally introduced into the EXAFS cell containing $Ir(C_2H_4)_2$/zeolite Y. The resultant XANES spectra (provided in the Supporting Information) showed a detectable increase in the white line intensity, suggesting that the XAS data would have allowed us to detect inadvertent oxidation of the iridium had that occurred during the shipping and handling.
(48) Lu, J.; Serna, P.; Gates, B. C. *ACS Catal.* **2011**, *1*, 1549−1561.
(49) Assignment of the contribution from hydrocarbon ligands on the basis of EXAFS spectroscopy is not straightforward, in part because of the possible presence of hydrocarbon rings which can be tilted and bent on top of the Ir atoms, causing the Ir−C and/or Ir−C_{long} contributions to be counted twice in some cases.
(50) Lu, J.; Aydin, C.; Liang, A. J.; Chen, C.-Y.; Browning, N. D.; Gates, B. C. *ACS Catal.* **2012**, *2*, 1002−1012.
(51) van't Blik, H. F. J.; van Zon, J. B. A. D.; Huizinga, T.; Vis, J. C.; Koningsberger, D. C.; Prins, R. *J. Am. Chem. Soc.* **1985**, *107*, 3139−3147.
(52) Fierro-Gonzalez, J. C.; Kuba, S.; Hao, Y.; Gates, B. C. *J. Phys. Chem. B* **2006**, *110*, 13326−13351.
(53) Davies, J. A.; Dutremez, S.; Pinkerton, A. A. *Inorg. Chem.* **1991**, *30*, 2380−2387.
(54) Tolman, C. A. *Chem. Rev.* **1977**, *77*, 313−348.
(55) Breck, D. W. In *Zeolite Molecular Sieves*; Krieger: Malabar, FL, 1984.
(56) Zahmakıran, M.; Tonbul, Y.; Özkar, S. *J. Am. Chem. Soc.* **2010**, *132*, 6541−6549.
(57) Hornstein, B. J.; Aiken, J. D., III; Finke, R. G. *Inorg. Chem.* **2002**, *41*, 1625−1638.
(58) Bayram, E.; Zahmakıran, M.; Özkar, S.; Finke, R. G. *Langmuir* **2010**, *26*, 12455−12464.